

bias

Bremer Institut für
angewandte Strahltechnik

Thermal Forming and Welding Distortion

F. Vollertsen, H. Tetzl (Eds.)

Proceedings of the IWOTE'14:
International Workshop on
Thermal Forming and
Welding Distortion



Analysis Techniques

H. Yunsook	
Analytical Methodology Obtaining an Optimal Welding Sequence for Least Distortion of Welded Structure.....	133
T. Loose, A. Patschger, J. Bliedtner	
Simulation-aided Optimization of a Laser-based Micro-welding Process.....	141

Welding Distortions

G.-H. Lee, H.-P. Cheon, S. J. Na	
CFD-Simulation of Welding Processes and its Application to Prediction of Welding Distortion	159
H. Koch, R. Goméz Vázquez, A. Otto	
Analysis of Distortion Effects on Weld pool Dynamics in Laser Beam Welding	165
S. Kohl, F. Hugger, V. Mann, M. Schmidt	
Towards numerical determination of distortion in laser welding	173
N. Osawa, J. Swamura, Y. Ikegami	
Study on the Relationship between the Heat Transfer Characteristics of Preheating Gas and Thermal Distortion in Oxyfuel Gas Cutting	185
M. San Sebastian, A. Ayesta, A. Mendizabal, E. Gorostegui, A. Echeverria	
Determination of the relationship between weld pool geometry and distortion field for electron beam welding process by means of numerical simulation.....	201

Thermal Forming

S. Gwynn-Jones, K. Hooman, B. Daniel	
Thermal Bending of Air Cooled Tubes	213
J. Griffiths, G. Sheikholeslami, S. Clark, S. P. Edwardson, G. Dearden	
Towards optimization of beam mode for high efficiency laser thermal forming within metallurgical constraints	233
W. J. Seong, S. J. Na	
A Study on an Inverse Solution to Flame Straightening by Geometrical Approach	243
M. Grden, N. Chopra, F. Vollertsen	
Laser beam bending of aluminum and stainless steel sheets at increased velocities.....	249
Author Index.....	259

Simulation-aided Optimization of a Laser-based Micro-welding Process

Tobias Loose¹, Andreas Patschger² and Jens Bliedtner²

¹ Ingenieurbüro Tobias Loose [engineering office], Herdweg 13, 75045 Wössingen (district of Karlsruhe), Germany

E-mail: loose@tl-ing.de

² Ernst-Abbe-Fachhochschule Jena [Jena University of Applied Sciences], Carl-Zeiss-Promenade 2, 07745 Jena, Germany

E-mail: Andreas.Patschger@fh-jena.de

ABSTRACT

In a research project with the purpose of resulting in an industrial application, a vacuum insulation panel is to be sealed using ultrathin CrNi steel foils. A laser beam joining process is applied to achieve the vacuum-tight sealing of the panel. In this context, laser-based micro-welding requires excellent process control due to the small material thicknesses of $\leq 50 \mu\text{m}$. So as to reliably weld the join partners to each other in the form of a lap joint, the process parameters need to be optimized.

The energy transported by the laser beam is partially absorbed and converted into heat. Hence, losses occur due to heat conduction into the component that are drawn from the actual process. The minimum material thickness of the steel foil, the process-related clamping length and the immanent compliance of the clamping means result in a reduced structural rigidity of the overall system that can absorb only small compressive stresses. While the component cools down, internal compressive stresses occur, causing the foils to buckle. The thermally induced distortion results in the formation of gaps between the join partners.

As heat conduction losses increase, distortion grows as well, and so does the joining gap, which causes the process to be interrupted. This implies an immediate impact on the joining process that is highly sensitive to vertical relative displacements of the foils. Hence, heat conduction losses and the associated distortion must be minimized.

The Péclet number is a measure of the relative portion of heat conduction losses in the laser-based machining process and is thus interrelated to thermal efficiency. The selected process parameters determine the Péclet number which is why they are critical when it comes to process reliability and joinability.

In order to qualify the impact, the process parameters are varied, and process efficiency is analyzed in dependence on the Péclet number. Experimental analysis is complemented by welding simulation enabling the calculation of global temperature field, internal stresses and distortion in dependence on the Péclet number and of the clamping length. The combination of experimental analysis and welding simulation is to help design a robust micro-joining process.

The component geometries used constitute a particular challenge in terms of the simulation. Based on the temperature field calculation, the heat introduction into the component can be derived, and the heated zone can be estimated. Both is crucial when it comes to the formation of distortions.

1 Introduction

The joint research project “CroNiVIP” (VP3018201AG2) of the ZIM [Zentrales Innovationsprogramm Mittelstand] is about the development of a new generation of innovative insulation elements. The primary objective is the development of novel vacuum insulation panels (VIP) with a thin, fully metallic CrNi steel foil envelope that exhibit excellent insulating properties on the one hand and fulfill high demands in terms of temperature stability on the other.

By substituting the conventional envelope material consisting of a multi-layer plastic film for a CrNi steel foil, the feasible application temperature range is extended far beyond the previous upper limit of 80°C.

This new property profile broadens the existing product range, thus opening up the opportunity to enter new market segments. Fields of application for the novel high-performance panels include, for example, solar-thermal applications, cryogenic engineering, furnace insulation and sensitive areas in terms of fire protection. [CroNiVIP project description, 2012]

The vacuum-tight sealing of the VIPs is to be performed by way of a laser beam joining process. A scanner-based remote process that can both guarantee a certain process speed and cover the working room as well is particularly suitable here. Since laser beam welding is still a thermal process despite its high efficiency, portions of the irradiated energy are conveyed into the component in the course of processing. This causes a thermally induced distortion resulting in the formation of a gap between the join partners. According to [Thomy et al., 2010], in case of a decreasing workpiece thickness d and a scaled energy input per unit length, thermally induced distortion Δz increases based on a power function.

$$\Delta z = \frac{1}{d^2} \quad (1)$$

That means that with the intended foil thicknesses of $\leq 50 \mu\text{m}$ there is a risk of process interruption due to an unbridgeable joining gap, which needs to be minimized. This can be achieved by way of adapted process control. According to [Beyer, 1996], the thermal losses can be described very well in dependence on the Péclet number. Hence, according to [Patschger et al., 2013], thermal efficiency follows from:

$$\eta_{th} = \frac{1}{1 + \left(\frac{Pe}{2}\right)^{-0.7}} \quad (2)$$

Degree of coupling η_{abs} and thermal efficiency together form the process efficiency η_{proc} :

$$\eta_{Proc} = \eta_{th} \cdot \eta_{abs} \quad (3)$$

In deep penetration welding, the degree of coupling is determined by the absorption coefficient A and the aspect ratio A_R . [Dausinger, 1995]

$$\eta_{abs} = A \cdot \frac{1 + (1 - A) \cdot \left[\frac{1}{2A_R} - \left(\frac{1}{2A_R} \right)^2 \right]}{A \cdot \left(1 - \frac{1}{2A_R} \right) + \frac{1}{2A_R}} \quad (4)$$

From formula 2 follows the necessity to design the process with a sufficiently high Péclet number. It is composed of feeding rate v , weld seam width b and thermal diffusivity κ [Poprawe et al., 2004]:

$$Pe = \frac{v \cdot b}{\kappa} \quad (5)$$

With a mostly specified material and thus defined thermal diffusivity κ , either focal diameter and weld seam width b or feeding rate v can be increased so as to increase Péclet number and process efficiency. In the case of micro-weld seams, the increase of the focal diameter is limited by the achievable minimum aspect ratios, while the speed can freely be increased up to the humping limit. High speed requires high power. When the heat conduction losses are subtracted, power linearly scales in relation to speed.

In order to demonstrate the difference in heat conduction loss with different feeding rates, two laser-based processing systems with clearly different power ranges and thus clearly different achievable speeds are used.

2 Experimental part of the analysis

2.1 Experimental setup and materials used

One disk laser system by the company PRENOVATEK and one fiber laser system by the company JENOPIK were used. They were both equipped with a RAYLASE beam deflecting unit. The technical data are shown below:

Table 1: Technical data of the laser-based material processing systems

		PRENOVATEK NovaDisc-P5	JENOPIK
System	-	Disk laser (DL)	Fiber laser (FL)
Max. power	W	40	1,000
Wavelength	nm	1,030	1,070
Beam propagation ratio M^2	-	1.2 [Strocka et al., 2012]	1.15 [Patschger et al., 2012]
Beam deflecting unit	-	RAYLASE Superscan-20	RAYLASE Superscan-LD30
Focal distance	mm	160	100
Focal diameter	µm	25 [Strocka et al., 2012]	22 [Patschger et al., 2012]

Both systems are comparable in terms of wavelength, beam quality and focal diameter. Hence, it can be assumed that the results are not influenced by different absorption coefficients or intensity distributions.

The examinations were performed using cold-rolled CrNi steel foils (1.4301) with thicknesses between 25 and 50 µm. For the determination of the Péclet number based on equation no. 5, thermal diffusivity was measured in cold-rolled thin sheets with a thickness of 500 µm, using a LINSEIS XFA 500 within a temperature range of up to 500°C (see Figure 1).

Thinner materials could not be used here due to the measurement method. The test specimens were procured from the same supplier. All data points shown in Figure 1 are based on each 3 measured values. The coefficient of determination R^2 of the regression line is 97 %. [Swift-Hook and Gick, 1973] suggest that a mean value is used for the examined temperature range $T_{Ambience}$

$< T < T_{Melt}$. From extrapolation applying the regression equation follows a thermal diffusivity value of 0.0463 cm²/s at an average process temperature of 715°C.

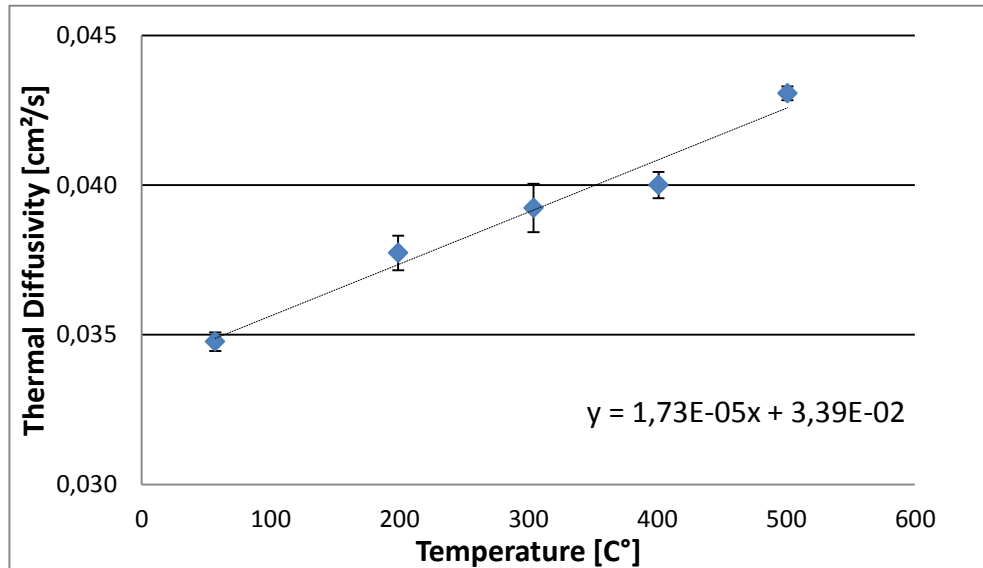


Figure 1: Thermal diffusivity in dependence on temperature

The weld seams were approx. 30 mm long, and the join partners were clamped using an aluminum fixture with a clamping length of approx. 6 - 8 mm.

2.2 Design and evaluation of the experiments

In aiming at keeping the theoretically achievable welding depth at a constant level during full penetration welding, only those data are taken into account in the evaluation of the examinations that were collected at the lower process boundary (see Figure 2).

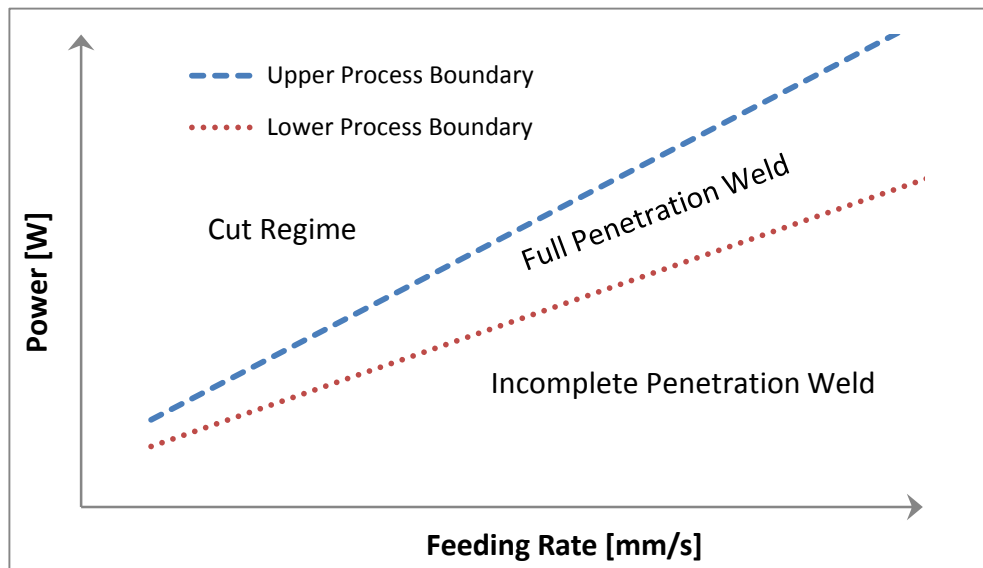


Figure 2: Simplified diagram to represent the process window

That means that at a constant power the speed was increased up to a point where an uninterrupted seam root was only just recognizable. This process was repeated at different lower levels, covering the complete power spectrum.

Implying that the lower process boundary is identical with a constant welding depth, the experiments involving identical foil thicknesses result in the same aspect ratio at nearly the same focal diameter and, thus, in the same degree of coupling. A constant degree of coupling allows direct conclusions about thermal efficiency from process efficiency (see equation no. 3).

2.3 Results and discussion

Specific energy per volume is a proven means to determine process efficiency. Since according to previous experimental series the degree of coupling for the respective foil thickness can be considered approximately constant, direct conclusions about thermal efficiency can be drawn from process efficiency.

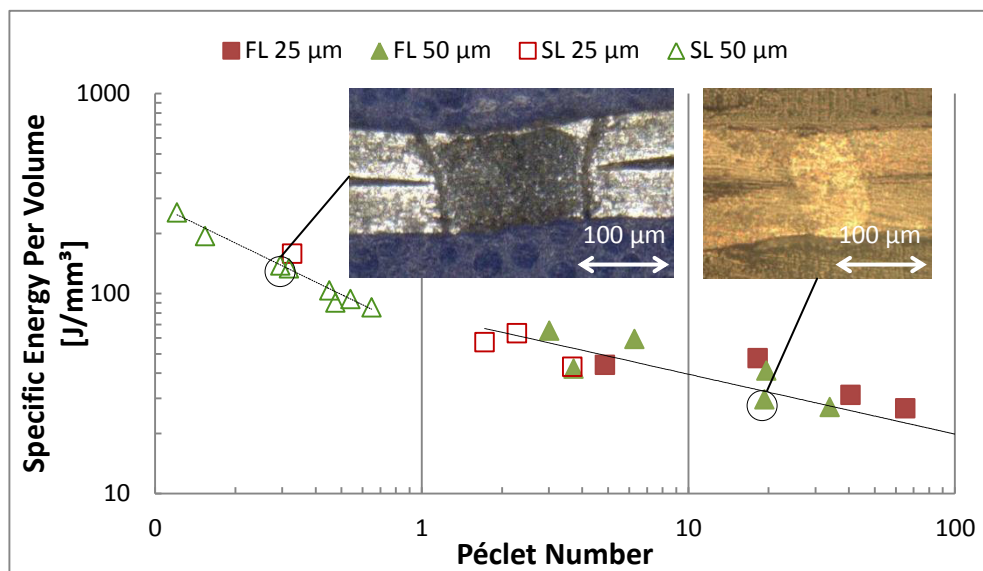


Figure 3: Specific energy per volume in dependence on the Péclet number

Figure 3 shows the specific energy per volume in dependence on the Péclet number for foil thicknesses of 25 µm and 50 µm, welded using the fiber laser (FL) and the disk laser (DL) system. The specific energy per volume steadily reduces as the Péclet number increases. That means that less and less energy needs to be introduced by the laser in order to melt the same volume. Hence, thermal efficiency grows as the Péclet number increases.

By way of the double logarithmic representation in Figure 3, the plotted functions are transformed graphically. Here, a power function forms a line. Thus, this type of representation can also be used as a test for power functions. [Stöcker, 2009] Figure 3 shows that exact behavior with the remarkable addition that in dependence on the Péclet number two regimes form that are subject to different thermal efficiencies. Moreover, Figure 3 implies that the threshold between the regimes equals a Péclet number of approx. 1. In order to verify this conclusion, the results are made subject to statistical regression analysis:

Table 2: Regression analysis results

	$Pe < 1$	$Pe > 1$
Coefficient of determination R^2	0.9434	0.7272
Gradient b	-0.64772	-0.2997
P -value for b	<0.001	<0.001
Upper boundary of 95 % confidence interval for b	-0.50587	-0.1843
Lower boundary of 95 % confidence interval for b	-0.78958	-0.4152
Intersection a	63.1361	78.884

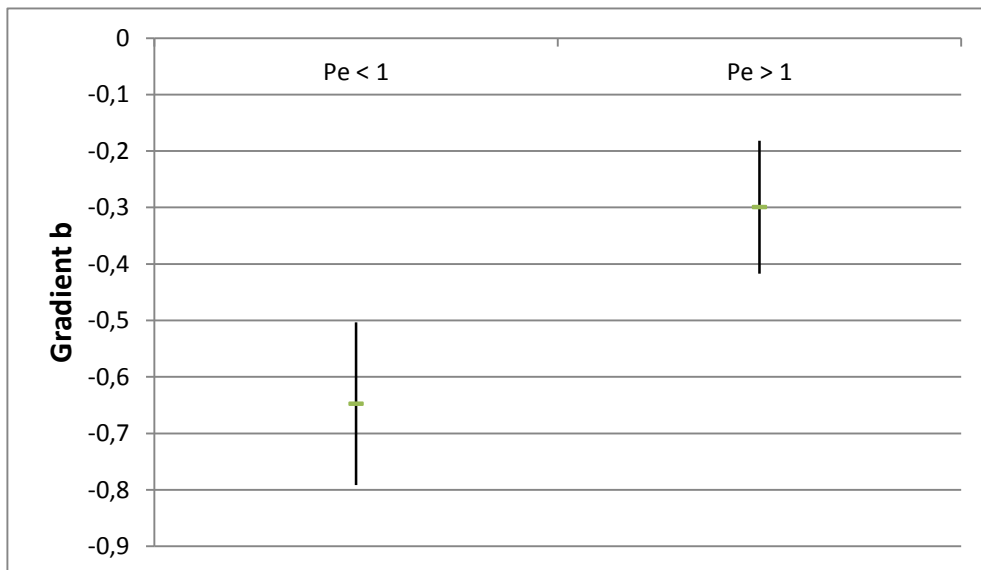


Figure 4: Gradient of the regression line with a 95 % confidence interval for different ranges of the Péclet number

Figure 4 shows clearly that the confidence intervals of the regression line gradients for Péclet numbers that are higher than 1 and lower than 1 do not overlap. A statistical comparison of the gradients based on the null hypothesis results in a significance value (P -value) of <0.001. Thus, the null hypothesis must be rejected in terms of the equality of the gradients. Hence, statistically, the gradients are significantly different. That means that where the Péclet number ranges above or below 1 respectively, thermal losses are subject to different dependencies as well as gradients. According to [Dausinger, 1995], different, theoretically determined ranges of the thermal efficiency for the Péclet number as per equation no. 5 are $Pe < 0.6$, $0.6 < Pe < 12$ and $Pe > 12$. Where the Péclet number exceeds 12, thermal efficiency reaches a maximal theoretical value of 48 %.

3 Simulative part of the analysis

3.1 Modeling

For the simulation, specimens of the welded 50 µm and 25 µm foils with different Péclet numbers were selected from both regimes (see Fig. 3).

Table 3: Process parameters of the specimens used

System	-	DL	FL	FL	DL	DL	FL	FL
Foil thickness	μm	50	50	50	25	25	25	25
Power (machining plane)	W	16.9	50	300	7.5	36	50	200
Feeding rate	mm/s	7.5	250	1,300	7.5	165	250	900
Nominal energy input per unit length	J/mm	2.25	0.20	0.23	1.00	0.22	0.20	0.22
Péclet number	-	0.32	3.67	19.3	0.33	3.67	4.87	18.3

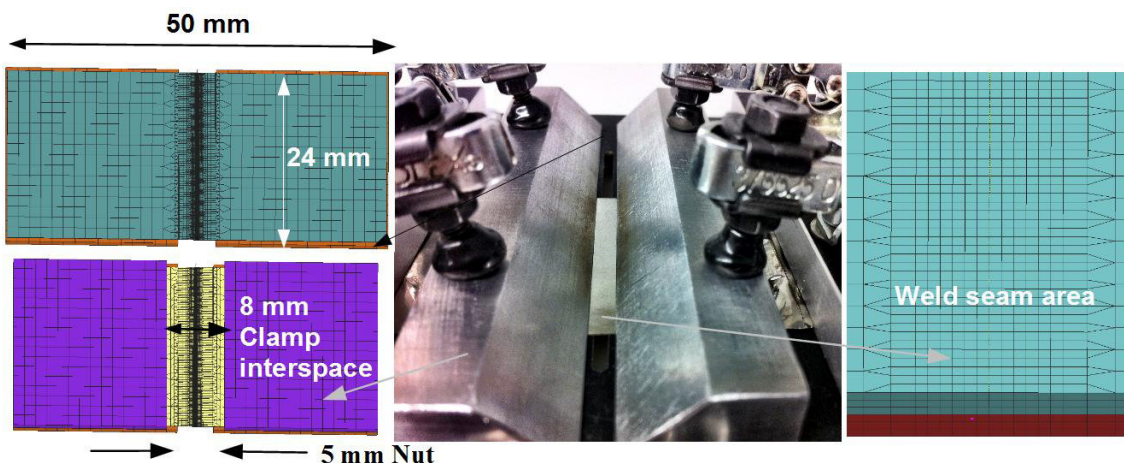


Figure 5: Experimental setup with clamping fixture and finite element model for transient calculation

Figure 5 shows the clamping situation in the experimental setup and the selected simulation in the finite element model with 3D volume elements. The seam area is cross-linked with three elements over the sheet thickness and an element edge length of 20 μm. The remote seam area, on the other hand, exhibits crosslinking with one element over the sheet thickness and an element edge length of 1,500 μm. This results in a model size of 152,410 elements. Heat transfer between clamping fixture bearing and foil and between clamping element and foil is assumed to be 100 W/(m²K). Heat transfer into the ambient atmosphere, on the other hand, is assessed to be 20 W/(m²K). The welding simulation was implemented using simufact.welding, versions 3.1.0 to 3.1.2, including the simufact Marc-Solver.

Computations are executed for two variant series:

Péclet number variant series

Heat introduction, and thus the Péclet number, is changed in accordance with the variants listed in table 3. The clamping situation is as shown in Figure 5.

Clamping length variant series

From the system characterized by 50 μm foil thickness and a Péclet number of 0.32, the heat introduction for the system characterized by 25 μm foil thickness is derived by dividing the power in half. Clamping length and notch width are varied with these two systems: 6 mm, 4 mm, 3 mm, 2 mm and 1.5 mm. In contrast to the clamping situation in Figure 5, clamping length and notch width are equal. The introduced heat always remains constant.

Heat introduction is not simulated, but predefined as an input parameter and realized by means of a substitute heat source. The latter is designed such that the same heat introduction as in the experiments is achieved. The performance data of the laser source alone are not sufficient here as the actual losses due to thermal conduction, reflection etc. are unknown. Applying the method of micrograph comparison, overall heat introduction into the metal sheet is determined by way of iteration. In this process, heat introduction is varied until the temperature field calculation results in the same weld pool cross-section as the micrograph.

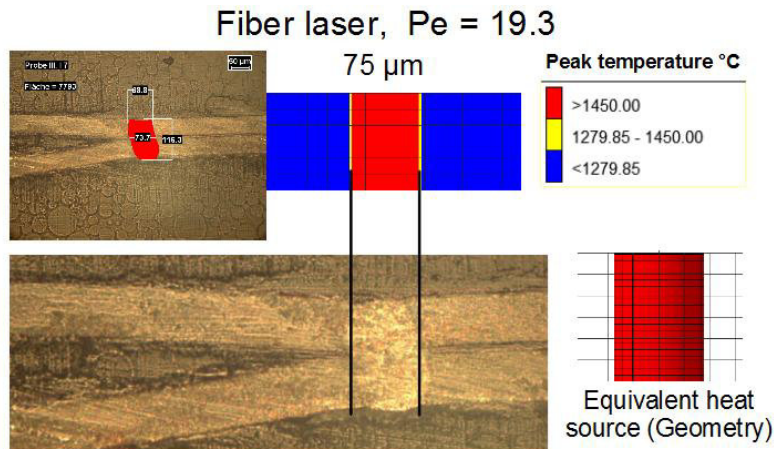


Figure 6: Micrograph comparison

Figure 6 shows the micrograph comparison for the specimen welded with the fiber laser system ($Pe = 19.3$). The substitute heat sources follow from the micrograph comparisons executed for all systems listed in table 3.

3.2 Material data

The temperature field calculation is done using the material data set from simufact.material 2012, X5CrNi18-10-sw, based on the dissertation published by [Voß, 2001], where the thermal conductivity values are modified. Basis for this are measurements of thermal diffusivity and thermal conductivity within a temperature range between 57°C and 501°C (see Figure 1). The supporting points at 20°C and 1,500°C are determined by way of extrapolation.

For the purpose of structural-mechanical calculation, the temperature-dependent stress-strain relation of the material data set is adapted in accordance with the results of hot tensile tests executed at the SLV Mecklenburg-Vorpommern [an educational establishment and research center] and then applied as shown in Figure 7. The hot tensile tests were performed using slightly hardened material with a thickness after rolling of 12 mm. The thin foils are significantly pre-hardened due to the very high degree of rolling down. Tensile tests carried through at the Jena University of Applied Sciences resulted in an elastic limit of 0.1 % at 1,050 N/mm². A plastic pre-hardening of 0.44 m/m was determined on that basis and defined as plastic initial strain in the finite element model of the foils. At 20°C, hardening increases in a strictly monotonic manner, while at higher temperatures, a slow-down of the hardening process can be observed after a maximum value has been reached. The latter is attributable to the creep behavior at high temperatures. This effect is not represented in the simulation data. The gradient of the line representing the hardening process was selected such that it is based on the hardening behavior observed at a temperature of 20°C.

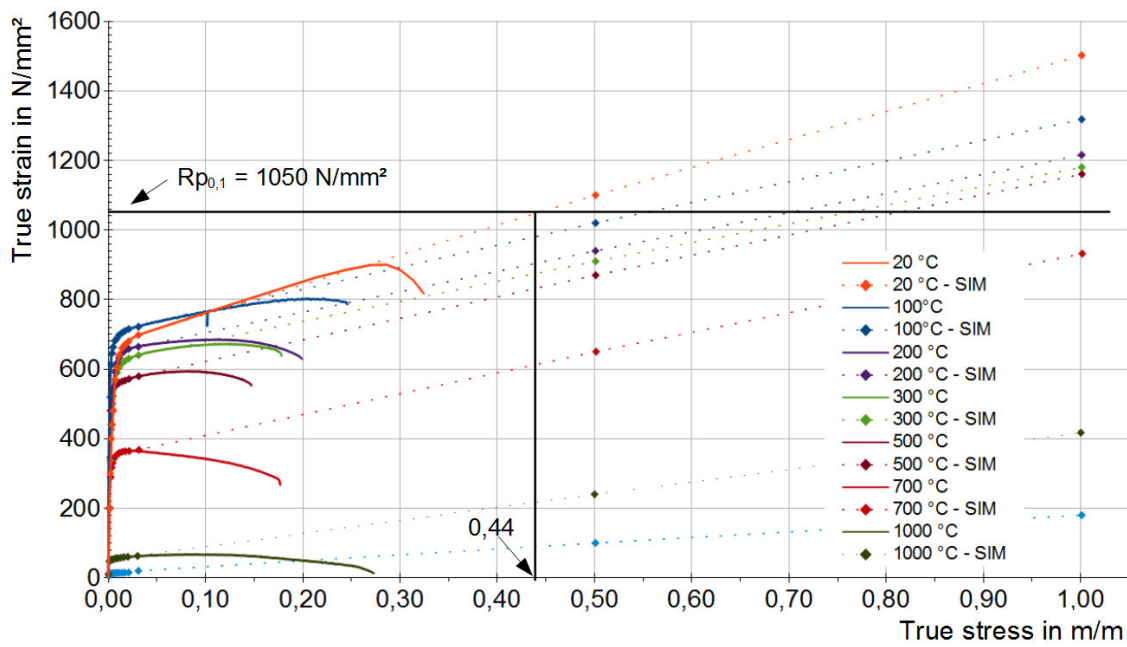


Figure 7: Stress-strain relation, hot tensile tests versus simulation data

3.3 Results of temperature field calculation

The temperature field calculation results have been published in [Patschger Loose et al., 2013].

Figure 8 shows the spatially resolved maximum temperature computed for the welding process, with a temperature resolution of up to 500°C at the surface of the welding specimen, for a foil thickness of 50 µm, with a very high Péclet number (19.3) and a very low Péclet number (0.32).

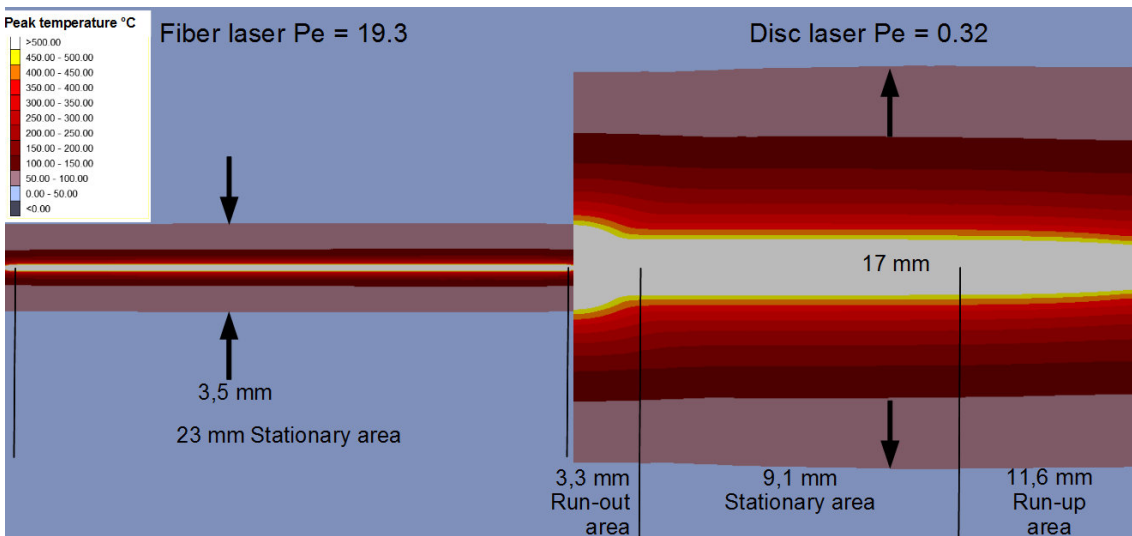


Figure 8: Maximum temperature in the welding process

With 3.5 mm, heat propagation during the welding process - measured based on the width of the 50°C isotherm - is much less during a welding process with a Péclet number of 19.3 than it is the case with a clearly smaller Péclet number where the 50°C isotherm is 17 mm wide. This area is called the heat-affected zone and has a significant impact on buckling [Vollertsen et al., 2007]. The smaller the heat-affected zone, the smaller the inherent forces, i.e. the internal tensile and compressive stresses across the sectional area. After the critical value is reached, internal compressive stresses can cause buckling and thus deformation perpendicularly to the foil thickness, leading to a process interruption due to the resulting formation of a gap between the join partners.

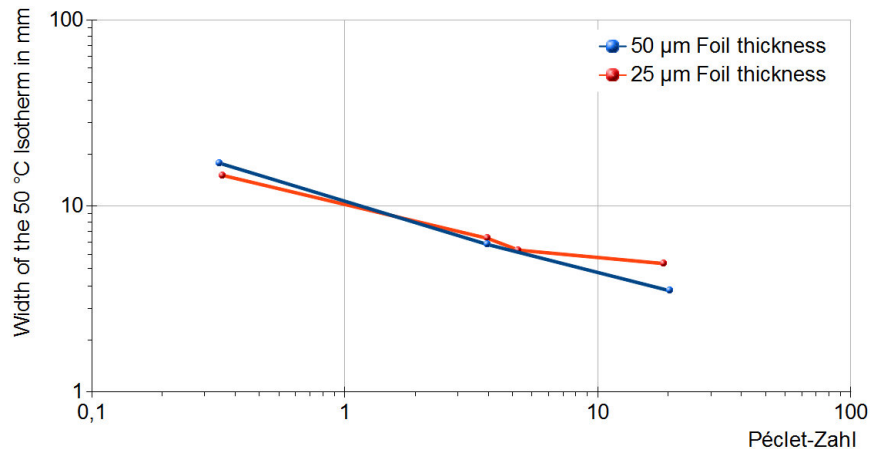


Figure 9: Width of the 50°C isotherm in dependence on the Péclet number and at a clamping length of 8 mm

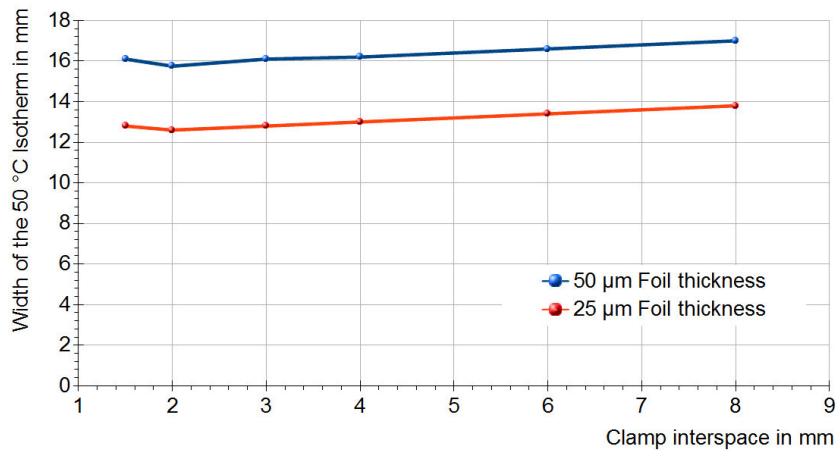


Figure 10: Width of the 50°C isotherm in dependence on the clamping length and at a Péclet number of 0.32

Figure 9 shows the width of the 50°C isotherm, plotted over the Péclet number. The course correlates with the relationship between Péclet number and specific energy per volume plotted in Figure 3. While heat propagation is significantly dependent on the Péclet number, the clamping length only has a minor impact on heat propagation.

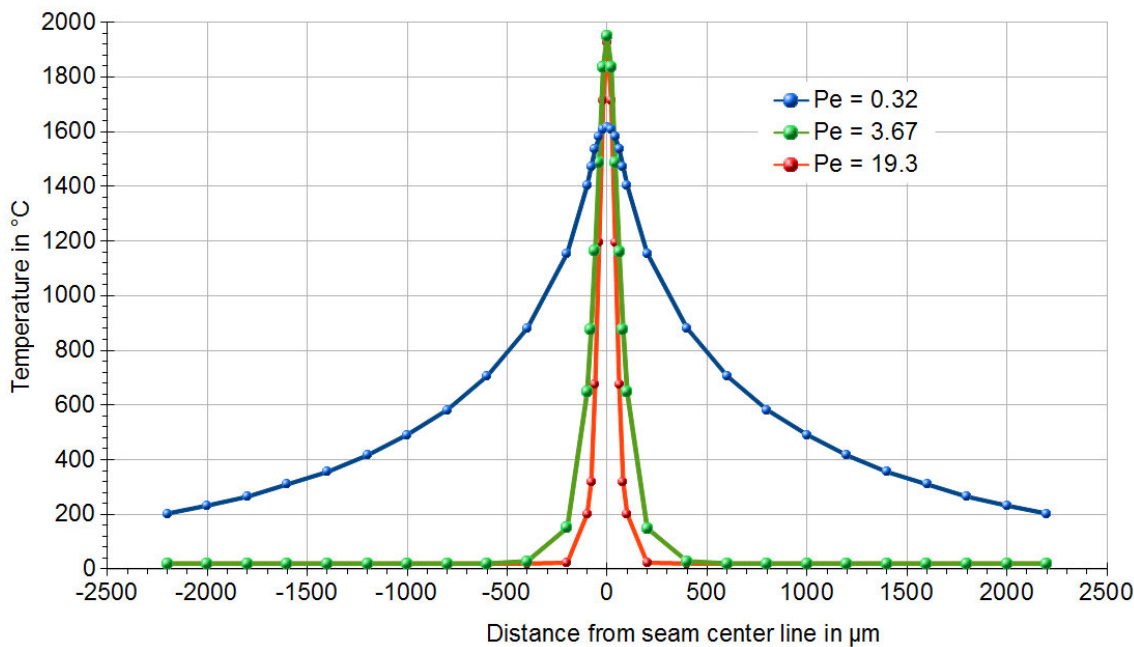


Figure 11: Temperature profile at focal passage in foil center, system: 50 μm foil thickness and 8 mm clamping length

Figure 11 shows the temperature profile of the heat-affected zone across the weld seam during the passage of the laser beam for various Péclet numbers on the example of 50 μm foils. A high Péclet number results in a narrow heated zone with a great temperature gradient across the weld seam, while the heated zone with a small Péclet number (disk laser) is much wider and exhibits a small temperature gradient.

The temperature integral is the temperature integrated over a certain reference length. In the case at hand, the reference length is a section on the specimen surface, running across the weld seam at the level of the focus line. The temperature integral of the curves shown in Figure 11 can be considered a measure of the introduced energy as well.

The overall temperature integral follows from the entire heated section within the 50°C isotherm. The weld pool temperature integral, on the other hand, is formed only over the section within the 1,500°C isotherm.

The actual welding process is limited to the fusing of the material within the weld seam cross-section. The heating of the adjacent areas draws energy from the joining process and can hence be considered lost heating. When relating the heating within the joining zone to the overall heating, the result will be the local or thermal efficiency.

Thermal efficiency can be described through the temperature integral by relating the weld pool temperature integral to the overall temperature integral. Table 4 compares those values based on different Péclet numbers. The significantly higher thermal efficiency associated with a high Péclet number is clearly recognizable. In this context, heating remains concentrated on the joining zone.

Table 5 shows that the clamping length does have an influence on thermal efficiency. The closer the clamps are to the weld seam, the more heat is dissipated into the clamps, and the smaller is

the thermal efficiency. However, the impact of the clamping length on thermal efficiency is not as considerable as that of the Péclet number.

Table 4: Temperature integral and thermal efficiency in dependence on the Péclet number, clamping length: 8 mm

Foil thickness	µm	50	50	50	25	25	25	25
Péclet number	-	0.32	3.67	19.3	0.33	3.67	4.87	18.3
Overall temperature integral	Kmm	3,025	368	214	3,211	484	378	138
Weld pool temperature integral	Kmm	276	141	129	166	134	142	56
Thermal efficiency	-	0.091	0.382	0.606	0.052	0.277	0.375	0.409

Table 5: Temperature integral and thermal efficiency in dependence on the clamping length, Péclet number: 0.32, foil thickness: 50 µm

Clamping length	mm	1,5	2	3	4	6	8
Overall temperature integral	Kmm	3,111	3,040	3,116	3,136	2,848	3,025
Weld pool temperature integral	Kmm	146	180	195	199	246	276
Thermal efficiency	-	0.047	0.059	0.063	0.064	0.086	0.091

3.4 Results of the structural-mechanical calculation

As soon as the first welds had been completed, deformations were observed in the weld seam area, forming orthogonally to the foil surface and taking the shape of a buckling pattern (Figure 12).

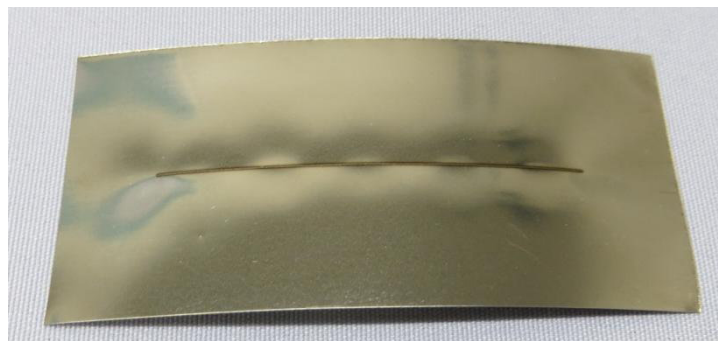


Figure 12: Condition of deformation after welding and cooling – experiment

This deformation is confirmed by the simulation (Figure 13). The buckling waves form during the welding process and are attributable to the strains caused by thermal heating. Figure 13 shows the vertical distortion at the end of the welding process and prior to cooling. The deformation has already developed. This remains qualitatively the case until the material has fully cooled down, with the amplitude decreasing due to temperature strain during the cooling process.

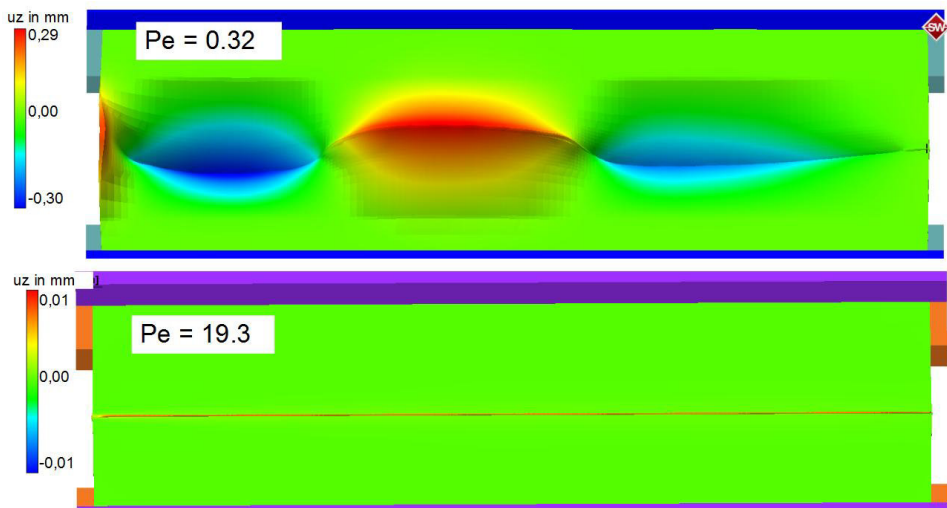


Figure 13: Vertical distortion after welding, exaggerated by a factor of 5, foil thickness: 50 µm, clamping length: 8 mm

The distortion that develops in the course of welding is directly dependent on the Péclet number. In addition to the fact that a small Péclet number results in major distortion, it is recognizable in Figures 11, 13 and 14 that the distortion is also clearly dependent on the heating of the areas adjacent to the weld seam. In the case of a Péclet number of 0.32, the areas adjacent to the weld seam are heated up to a great extent, and a significant buckling pattern develops. In the case of a Péclet number of 19.3, nearly only the weld seam area itself is heated up. No buckling pattern with considerable deformation amplitudes is formed, but merely a slight upsetting deformation within the weld seam area. Above the Péclet number, Figure 14 shows the deformation amplitude and the number of buckling waves forming over the model width of 24 mm. At a certain Péclet number, the distortion pattern changes from the wavy buckling shape to linear upsetting deformation. This critical Péclet number is dependent on system rigidity. The lower the rigidity of the system, the higher the critical Péclet number. Figure 13 shows that with the 25 µm foil the transition to the linear upsetting deformation is shifted to the right, in the direction where the Péclet number gets higher.

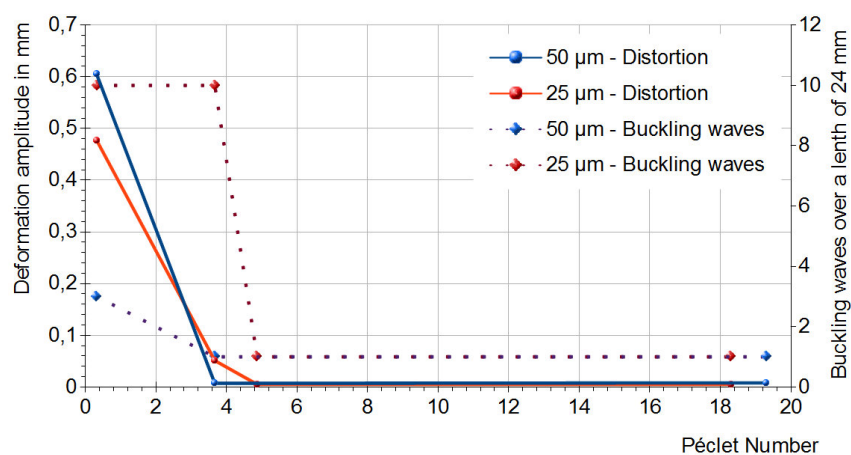


Figure 14: Number of buckling waves and deformation amplitude in dependence on the Péclet number and at a clamping length of 8 mm

Buckling shapes are determined by the intrinsic values of a system and are dependent on system rigidity and clamping length. This mechanism is obvious in the thin-film welding process observed. Hence, foil thickness has an immediate impact. In Figure 15 the distortion shapes of 25 µm and 50 µm foils at a clamping length of 3 mm are compared to each other. While the 25 µm foil clearly shows buckling, the transition to linear upsetting deformation is already recognizable with the 50 µm foil.

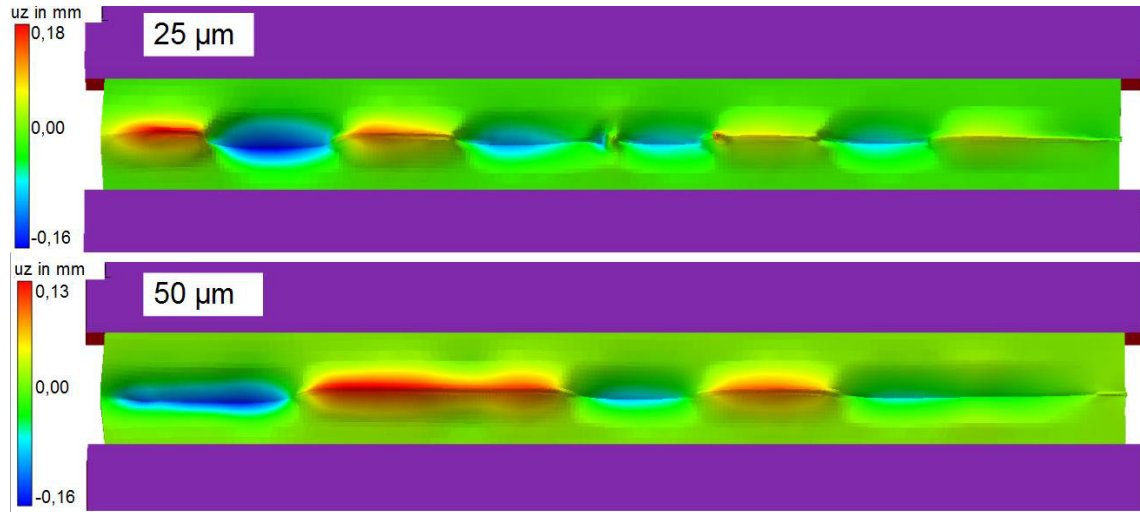


Figure 15: Vertical distortion after welding, exaggerated by a factor of 5, Péclet number: 0.32, clamping length: 3 mm

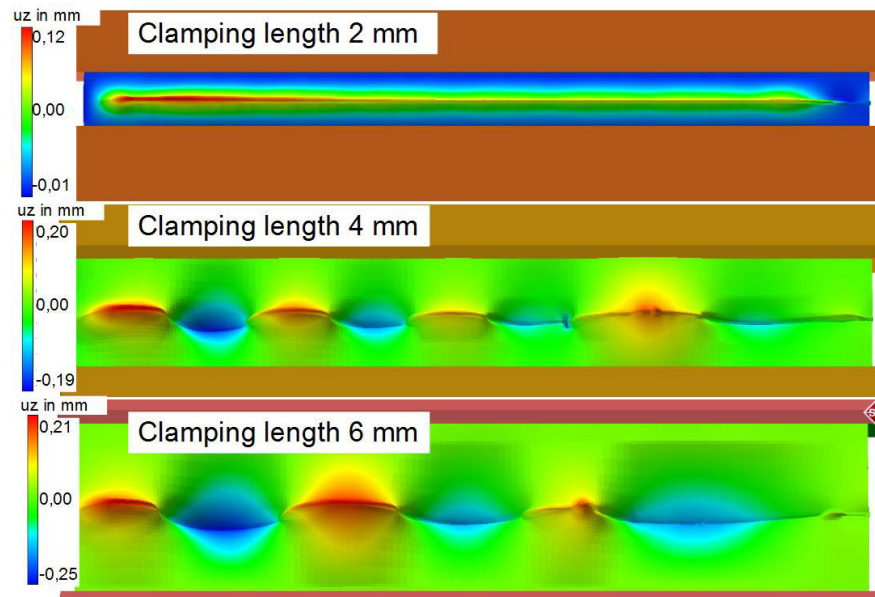


Figure 16: Vertical distortion after welding, exaggerated by a factor of 5, foil thickness: 25 µm, Péclet number: 0.32

Figure 16 shows the form of distortion with the 25 µm foil for three different clamping lengths: 2 mm, 4 mm and 6 mm. System rigidity depends on both foil thickness and clamping length. Consequentially, the form of distortion must be dependent on the clamping length as well. With a

clamping length of 2 mm a linear upsetting deformation develops, while from a clamping length of 3 mm the buckling form appears.

Figure 17 shows the number of buckling waves plotted over the model length and the deformation amplitude over the clamping length. At a critical clamping length that is dependent on the foil thickness, the shape of distortion changes from a linear upsetting deformation to buckling. Furthermore, the deformation amplitude rises as the clamping length grows.

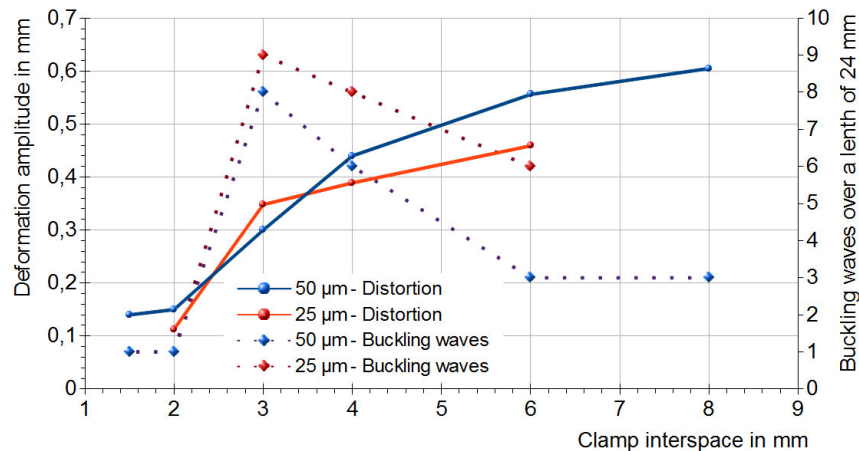


Figure 17: Number of buckling waves and deformation amplitude in dependence on clamping length, Péclet number: 0.32

The distortion that develops in the course of welding puts the process at risk. So far, the simulations resulted in a unidirectional deformation of both foils. However, it is absolutely possible for the foils to move apart as the buckling develops, thus forming a gap that would jeopardize the process. Hence, when it comes to ensuring process stability, it can be stated that the greatest possible system rigidity is to be aimed at, i.e. smallest possible clamping length and greatest possible Péclet number.

4 Summary and conclusions

In order to ensure a reliable production process, disturbances such as gap formation due to thermal deformation must be minimized.

The distortion is caused by internal strains. It develops when the material is heated up during welding. Certain areas within the heat-affected zone are made subject to thermal strain and give way normal to the foil plane.

The width of the heat-affected zone scales with the Péclet number. The higher the Péclet number, the smaller the heat-affected zone.

Thermal efficiency, i.e. the relationship of the energy introduced to melt the material in the area of the weld metal to the overall energy introduced into the component, scales with the Péclet number as well. The higher the Péclet number, the greater the thermal efficiency.

The degree of clamping, i.e. the free length between the clamps, also has a direct influence on distortion. The greater the degree of clamping, the greater the distortion.

Moreover, the clamping length also has a certain, albeit minor, impact on thermal efficiency. The greater the clamping length, the greater the thermal efficiency.

Two different forms of distortion can develop: Linear yielding or checkered buckling. The number of buckling waves per weld seam length depends on the clamping length. The greater the clamping length, the less buckling waves per unit length.

The transition of the distortion pattern from checkered buckling to linear yielding depends on a critical Péclet number that needs to be exceeded, a critical clamping length that needs to be undercut, or a critical foil thickness that needs to be exceeded. In this context, these three parameters are interdependent.

In order to design a reliable process, the distortion that develops in the course of welding must be minimized. This can be achieved when:

- the greatest possible Péclet number is achieved.
- the clamping length is minimized.

5 Acknowledgements

The authors would like to thank the BMWi [German Federal Ministry for Economic Affairs and Energy] for funding this research and AIF e.V. [German Federation of Industrial Research Associations] for the support. (VP3018201AG2)

6 References

- N.N. (2012): Projektbeschreibung *Entwicklung eines neuartigen, mechanisch belastbaren Vakuum-Isolations-Panels mit breitem Einsatzspektrum für Hochleistungsanwendungen durch Verwendung einer CrNi-Stahlhülle* [Project description. *Development of a novel vacuum insulation panel that can resist mechanical stress and has a broad spectrum of use in high performance applications by using a CrNi steel envelope*] (CroNiVIP) (VP2156309AG2).
- Beyer, E. (1995): *Schweißen mit dem Laser – Grundlagen* [Welding with the Laser – Basics], Springer-Verlag publishing house, Berlin, Heidelberg, New York, p. 138.
- Dausinger, F. (1995): *Strahlwerkzeug Laser: Energieeinkopplung und Prozeßeffektivität* [The Laser as a Beam Tool: Energy Coupling and Process Efficiency], habilitation, University of Stuttgart, B.G. Teubner Verlag publishing house, Stuttgart, p. 34, p. 87.
- Patschger, A., Bergmann, J.P., Bliedtner, J. (2012): "Flexible and Efficient Laser Remote Welding of Ultra-thin Metal Foils", *J. Laser Appl.* 24, 052005.
- Patschger, A., Bliedtner, J., Bergmann, J.P. (2013): "Approaches to Increase Process Efficiency in Laser Micro Welding", *Physics Procedia*, volume 41, p. 585-595, ISSN 1875-3892.
- Patschger, A., Loose, T., Bliedtner, J. (2013): "Simulationsgestützte Prozessoptimierung eines laserbasierten Mikroschweißverfahrens" ["Simulation-aided Optimization of a Laser-based Micro-welding Process"], *Simulation Forum on Welding and Heat Treatment 2013*.
- Poprawe, R., Weber, H., Herziger, G. (Ed.) (2004): *Landolt-Börnstein Numerical Data and Functional Relationships in Science and Technology*, New Series / Group VIII: Advanced Materials and Technologies, volume 1, Laser Physics and Applications, subvolume C: Laser Applications: Fundamentals of Laser-induced Processes, Springer, Berlin, Heidelberg, New York, p. 61.

Strocka, S., Hopf, A., Patschger, A., Bliedtner, J., Hild, M., Störzner, F. (2012): "Beitrag zur Prozessentwicklung für das Remote-Laser-Schweißen von dünnen metallischen Folien" ["Contribution to Process Development for Remote Laser Welding of Thin Metallic Foils"], 22. Internationale Wissenschaftliche Konferenz Mittweida [22nd International Scientific Conference in Mittweida], Mittweida, Germany.

Stöcker, H. (2009): *Taschenbuch mathematischer Formeln und moderner Verfahren [Pocket Book of Mathematical Formulas and Modern Procedures]*, 4th edition, Harri Deutsch Verlag publishing house, Frankfurt am Main, p. 149.

Swift-Hook, D.T., Gick, A.E.F. (1973): "Penetration Welding with Lasers", *Weld. Res.* 52, p. 492-499.

Thomy, C., Möller, F., Vollertsen, F. (2010): "Distortion effects in micro welding with fibre laser", *Proc. of ICALEO, 29th int. Cong. On Applications of Lasers and Electro-Optics*, Anaheim, USA, LIA Publication 613 (CD), 301, p. 85-90.

Vollertsen, F., Wagner, F., Thomy, C. (2007): "Micro welding for environmental-friendly products", *Proc. of ICALEO, 26th int. Cong. On Applications of Lasers and Electro-Optics*, Orlando, USA, LIA Publication 610 (CD), 308, p. 143-148.

Voß, O. (2001): *Untersuchung relevanter Einflußgrößen auf die numerische Schweißsimulation [Examination of Relevant Parameters Influencing Numerical Welding Simulations]*, dissertation, Technische Universität Braunschweig.